Diagnostic Study

INTERNATIONAL JOURNAL OF SURGERY

OPEN

A multi-modal model integrating MRI habitat and clinicopathology to predict platinum sensitivity in patients with high-grade serous ovarian cancer: a diagnostic study

Qiu Bi, MD[a,b], Conghui Ai, MD[c], Qingyin Meng, MM[d], Qinqing Wang, MM[e], Haiyan Li, BM[b], Ao Zhou, MM[f], Wenwei Shi, MD[g], Ying Lei, MM[g], Yunzhu Wu, PHD[g,h], Yang Song, PHD[i], Zhibo Xiao, MD[f,*], Haiming Li, MD[j,*], Jinwei Qiang, MD[a,*]

Background: Platinum resistance of high-grade serous ovarian cancer (HGSOC) cannot currently be recognized by specific molecular biomarkers. We aimed to compare the predictive capacity of various models integrating MRI habitat, whole slide images (WSIs), and clinical parameters to predict platinum sensitivity in HGSOC patients.

Methods: A retrospective study involving 998 eligible patients from four hospitals was conducted. MRI habitats were clustered using K-means algorithm on multi-parametric MRI. Following feature extraction and selection, a Habitat model was developed. Vision Transformer (ViT) and multi-instance learning were trained to derive the patch-level prediction and WSI-level prediction on hematoxylin and eosin (H&E)-stained WSIs, respectively, forming a Pathology model. Logistic regression (LR) was used to create a Clinic model. A multi-modal model integrating Clinic, Habitat, and Pathology (CHP) was constructed using Multi-Head Attention (MHA) and compared with the unimodal models and Ensemble multi-modal models. The area under the curve (AUC) and integrated discrimination improvement (IDI) value were used to assess model performance and gains.

Results: In the internal validation cohort and the external test cohort, the Habitat model showed the highest AUCs (0.722 and 0.685) compared to the Clinic model (0.683 and 0.681) and the Pathology model (0.533 and 0.565), respectively. The AUCs (0.789 and 0.807) of the multi-modal model interating CHP based on MHA were highest than those of any unimodal models and Ensemble multi-modal models, with positive IDI values.

Conclusion: MRI-based habitat imaging showed potentials to predict platinum sensitivity in HGSOC patients. Multi-modal integration of CHP based on MHA was helpful to improve prediction performance.

Keywords: habitat, MRI, ovarian cancer, pathology, platinum sensitivity

Introduction

Ovarian cancer (OC) is recognized as an especially lethal type of gynecological malignancy, ranking sixth in terms of mortality rates within the female demographic[1]. OC includes several histological subtypes, with high-grade serous ovarian carcinoma (HGSOC) being the most common and aggressive[2]. HGSOC accounts for most OC-related deaths and is typically diagnosed at an advanced stage due to the lack of reliable screening methods for early

[a]Department of Radiology, Jinshan Hospital, Fudan University, Shanghai, China, [b]Department of MRI, the First People's Hospital of Yunnan Province, the Affiliated Hospital of Kunming University of Science and Technology, Kunming, YN, China, [c]Department of Radiology, Yunnan Cancer Hospital, the Third Affiliated Hospital of Kunming Medical, University, Peking University Cancer Hospital Yunnan, Kunming, YN, China, [d]Department of Pathology, Yunnan Cancer Hospital, the Third Affiliated Hospital of Kunming Medical University, Peking University Cancer Hospital Yunnan, Kunming, YN, China, [e]Department of Pathology, the First People's Hospital of Yunnan Province, the Affiliated Hospital of Kunming University of Science and Technology, Kunming, YN, China, [f]Department of Radiology, the First Affiliated Hospital of Chongqing Medical University, Chongqing, China, [g]Department of Radiology, Zhongda Hospital, School of Medicine, Southeast University, Nanjing, JS, China, [h]Institute for AI in Medicine, School of Artificial Intelligence, Nanjing University of Information Science and Technology, Nanjing, JS, China, [i]MR Research Collaboration Team, Siemens Healthineers Ltd, Shanghai, China and [j]Department of Radiology, Fudan University Shanghai Cancer Center, Shanghai, China; Department of Oncology, Shanghai Medical College, Fudan University, Shanghai, China

Qiu Bi, Conghui Ai, Qingyin Meng, and Qinqing Wang have contributed equally to this work and share first authorship.

*Corresponding authors. Address: Department of Radiology, the First Affiliated Hospital of Chongqing Medical University, No. 1 Youyi Road, Yuanjiagang, Yuzhong District, Chongqing 400016, China. Tel.: +86 13018380969. E-mail: 5894526@qq.com (Z. Xiao); Department of Radiology, Fudan University Shanghai Cancer Center; Department of Oncology, Shanghai Medical College, Fudan University, No.270 Dongan Road, Xuhui District, Shanghai 200032, China. Tel.: +86 18121299411. E-mail: lihaiming0109@163.com (H. Li); Department of Radiology, Jinshan Hospital, Fudan University, No.1508 Longhang Road, Jinshan District, Shanghai 201508, China. Tel.: +86 18930819898. E-mail: qiangjinwei@fudan.edu.cn; dr.jinweiqiang@163.com (J. Qiang).

International Journal of Surgery (2025) 111:4222–4233

Received 15 January 2025; Accepted 2 May 2025

Supplemental Digital Content is available for this article. Direct URL citations are provided in the HTML and PDF versions of this article on the journal's website, www.lww.com/international-journal-of-surgery.

Published online 20 May 2025

http://dx.doi.org/10.1097/JS9.0000000000002524

detection[3]. Despite initial therapy, usually consisting of surgical cytoreduction followed by systemic platinum-based chemotherapy after surgery, up to 70% of patients with advanced-stage HGSOC will relapse within 3 years[4,5]. Thereinto, platinum resistance accounts for approximately 15% of relapses[6]. Due to response of platinum-based chemotherapy cannot currently be recognized by specific molecular biomarkers[4], it is urgently necessary to explore alternative methods to predict platinum resistance in HGSOC patients.

Magnetic resonance imaging (MRI) and its functional imaging such as diffusion-weighted imaging (DWI) have the potential to predict the therapeutic response of OC[7,8]. With the development of artificial intelligence, radiomics, and deep learning based on MRI have gradually been applied to predict response of platinum-based chemotherapy in OC patients[9-11]. Notwithstanding radiomics and deep learning are capable of extracting quantitative and high dimensional features from tumor images, they cannot precisely reflect the tumor heterogeneity and microenvironment. Habitat imaging, a data-driven image processing technique that divides the entire lesion into multiple sub-regions without assuming anything prior, has capacity to non-invasively evaluate the intratumoral heterogeneity[12-14]. A previous study found that habitat radiomics based on PET/CT was associated with the expression of Ki-67 and prognosis in HGSOC patients[15], preliminarily suggesting that habitat radiomics was of certain significance for the assessment of HGSOC.

Many diseases are diagnosed and treated based on the histopathological morphology analysis, which is labor-intensive and subjective[16]. Pathomics, a combination of histopathology and artificial intelligence, enables comprehensive quantitative pathology data mining, and the pathomics based on hematoxylin and eosin (H&E)-stained whole slide images (WSIs) has shown potential to predict platinum resistance in OC patients[17-19]. A recent study discovered that integrated machine learning models based on CT images, clinical, pathological, and genomic features were able to effectively improve risk stratification of HGSOC[20]. Multi-modal integration may have more potential for accurate prediction of platinum resistance in HGSOC patients. However, different modalities reflect the state of the disease from different scales, and conventional integrated algorithms are limited in their ability to capture the features of various omics. Multi-head attention (MHA) mechanism can integrate features at different levels and assign weights to each feature, thus improving the accuracy of the model[21]. In this study, we aimed to develop and validate a MHA-based multi-modal model of Clinic, Habitat, and Pathology (CHP) to predict platinum sensitivity in HGSOC patients and compared with the unimodal models and Ensemble multi-modal models, aiming to provide multi-scale insights into tumor heterogeneity and treatment response.

HIGHLIGHTS

- Habitat imaging based on MRI was associated with platinum sensitivity in high-grade serous ovarian cancer (HGSOC) patients.
- The Clinic, Habitat, and Pathology (CHP) models had some potentials to predict platinum resistance of HGSOC patients, and the prediction performance of the Habitat model were better than that of the Clinic and Pathology models.
- The multi-modal model of CHP based on multi-head attention successfully predicted the platinum sensitivity and exhibited higher and more stable predictive performance than other models.

Methods

Patients

The work has been reported in line with the STARD (Standards for the Reporting of Diagnostic accuracy studies) criteria[22]. Between May 2015 and October 2023, all eligible patients from Hospital A were retrospectively enrolled as the training cohort and internal validation cohort in a ratio of 7:3, while the eligible patients from Hospitals B, C, and D were retrospectively designated as the external test cohorts. The process of patient selection is presented in Fig. 1. The inclusion criteria included: (a) patients diagnosed as HGSOC based on surgery and pathology; (b) the standard treatment including surgical cytoreduction followed by at least three cycles of regular platinum-based chemotherapy after surgery; (c) follow-up records available for more than 6 months after postoperative chemotherapy; and (d) for MRI analysis, pelvic MRI examination including axial T2-weighted imaging (T2WI), contrast-enhanced T1-weighted imaging (CE-T1WI), and DWI was performed within 2 weeks prior to treatment, and patients had no any treatments other than neoadjuvant chemotherapy (NACT) performed between MRI and surgery. The exclusion criteria included: (a) patients with a history of platinum-based chemotherapy for other malignancies; (b) absence of essential clinical data; (c) for MRI analysis, patients with poor MRI imaging quality and registration, or a tumor maximum diameter <1 cm on MRI needed to be excluded; and (d) for pathology analysis, patients without H&E-stained WSIs or with poor WSI imaging quality should be excluded. The final study population consisted of 998 eligible patients, of whom 578 patients had available clinical and MRI data, 587 patients had clinical and WSI data, 16 patients had clinical data only, and 183 patients had clinical, MRI, and WSI data. Patients from hospitals C and D were unable to access WSI data. The collection and processing procedures for clinical, MRI, and WSI data across all cohorts were consistent.

Clinic model construction

The clinical and pathological structured parameters of HGSOC patients included: general information, hospital records, diagnosis and treatment details, laboratory data, surgical and histopathological findings, immunohistochemical staining, and follow-up information. Platinum sensitivity is determined based on whether there is disease progression during or within 6 months after termination of platinum-based chemotherapy[23]. Patient follow-up starts from the date of admission and ends with the occurrence of an outcome event, loss to follow-up, or the end of the follow-up period. Although the start dates varied, all patients were followed up until May 2024 or death. In the training cohort, univariate and multi-variate logistic regression (LR) analyses were conducted to

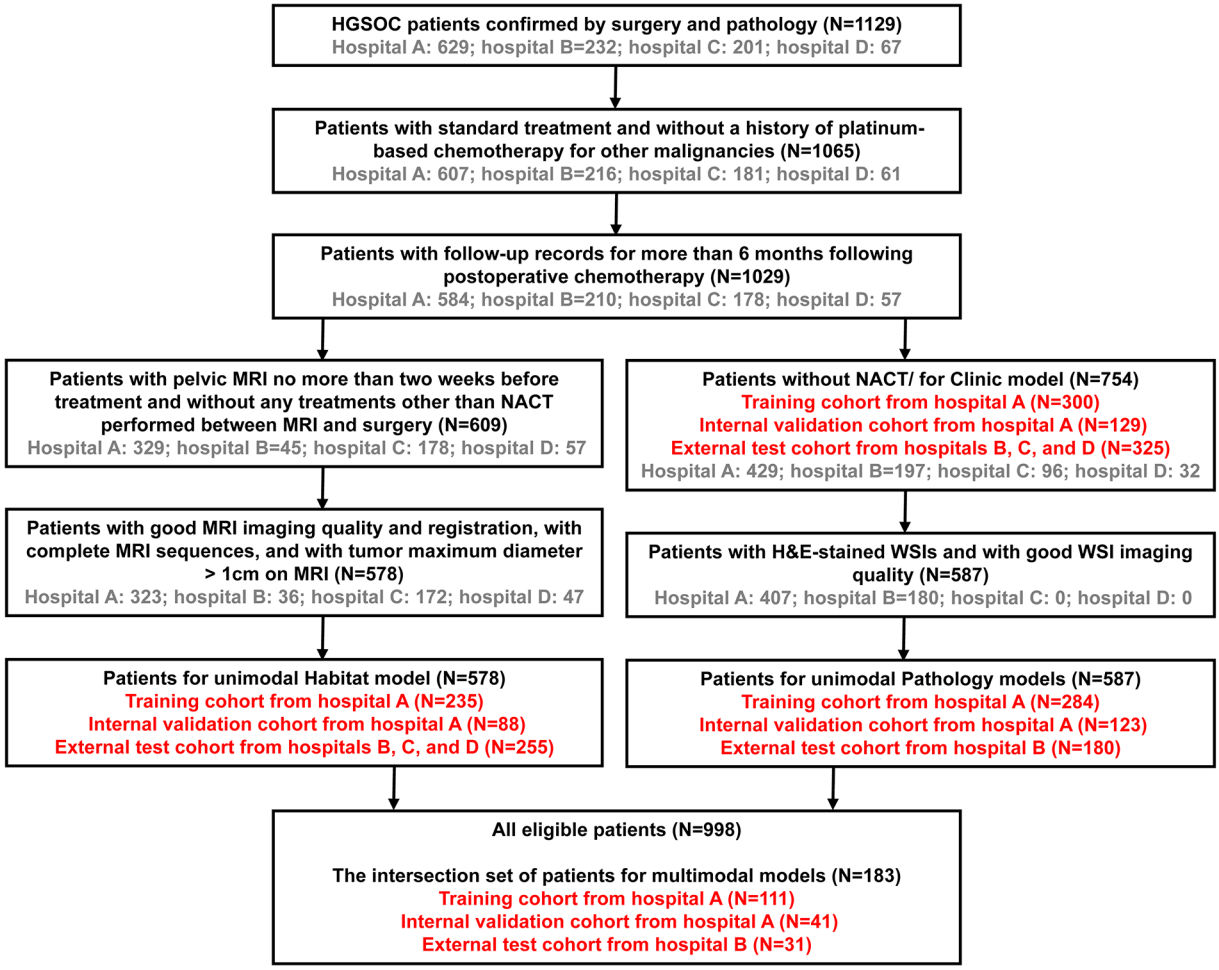

Figure 1. The process of patient selection. HGSOC: high-grade serous ovarian cancer; NACT: neoadjuvant chemotherapy; H&E: haematoxylin and eosin; WSI: whole slide image.

identify clinical independent predictors and construct the Clinic model.

MRI acquisition and habitat clustering

Pelvic MRI examinations were performed using 1.5-T or 3.0-T scanners. Supplementary Table S1 (http://links.lww.com/JS9/E191) lists details on MRI devices and parameter of the critical sequences. Depending on the patient's individual differences, partial parameters were adjusted. After image preprocessing and lesion segmentation, MRI habitats were clustered. Detailed information on MRI image preprocessing and segmentation is presented in Supplementary Note 1 (http://links.lww.com/JS9/E191).

The sequences that need to be clustered included: T2WI, CE-T1WI at venous phase, DWI, and apparent diffusion coefficient (ADC) maps. K-means clustering algorithm based on cohort (https://scikit-learn.org/stable/index.html) was applied to cluster MRI habitat sub-regions. The squared Euclidean distance between voxel intensities was used as the clustering cost measure. We employed Calinski–Harabasz score to determine the best number of clusters that were tested from two to ten in this study. The mean signal intensity (SI), volume, and proportion of different habitat on multi-parametric MRI were calculated.

Habitat feature extraction and selection

Habitat features were extracted from each sub-region using the Pyradiomics (https://pypi.org/project/pyradiomics/). Detailed information on habitat feature extraction and selection is provided in Supplementary Note 2 and Fig. S1 (http://links.lww.com/JS9/E191). After feature extraction, we performed *Z*-score to standardize the features in all cohort. Then *t*-test, Pearson correlation analysis, minimum redundancy maximum relevance, and the least absolute shrinkage and selection operator (LASSO) regression were applied sequentially for feature reduction and selection in the training cohort.

Habitat model construction

The common classifiers such as LR, Extra Trees, Random Forest, Naive Bayes, support vector machine (SVM), K nearest neighbor (KNN), eXtreme Gradient Boosting (XGBoost), and Light Gradient Boosting Machine (LightGBM) were used to construct habitat models based on sub-regions. The optimal hyper-parameter was determined by applying a five-fold cross-validation strategy coupled with a Grid-search algorithm. We performed 1000 bootstraps of the entire construction process to ensure the model's robustness. In different machine learning algorithms, the

optimal algorithm with high performance and strong generalization ability was employed as the Habitat model.

WSI acquisition and preprocessing

All tissue samples from hospitals A and B were collected after primary debulking surgery. Embedding in immunohistochemistry-grade paraffin was performed after samples had been soaked in 10% formalin for 4 hours. Afterward, the samples were sectioned at 4-μm intervals and stained with H&E for pathological analysis. Each H&E-stained slide contained one to three pieces of tissue. After removing the slices with heavy impurity, uneven staining, and tissue deformation, two senior pathologists (both with 18 years of experience in gynecologic pathological diagnosis) evaluated all H&E-stained slides for each patient and selected one slide with the richest tumor area for further analysis. One of the pathologists scanned the selected H&E-stained slides using a digital whole-slide scanner (SUNPA MIP 1500) at 20× objective lens to obtain WSIs for each patient.

Due to the extremely large size of WSIs, the images in all cohorts were divided into 512 × 512-pixel non-overlapping patches at 20× magnification for subsequent analysis. After removing the empty patches with no tissue, we used the Macehko method[24] to achieve staining normalization of the remaining patches in all cohorts. The Z-score on RGB channels was used to normalize the image intensity in all cohorts. Online data augmentations including random flipping and random transformation were applied during the training.

Pathology model construction

The pipeline encompassed two levels of predictions: patch and WSI. To address the challenges of large image size, we initially partitioned each WSI into smaller patches. The WSI-level prediction was then derived using an ensemble algorithm that amalgamated patch likelihoods. For the patch-level prediction, we harnessed the Vision Transformer (ViT) model[25,26] to train the patches. The architecture of ViT is given in Fig. 2a. The ViT model eliminates the use of recurrence, opting instead to rely exclusively on an attention mechanism to establish global dependencies between input and output. In contrast to convolutional neural networks, the ViT model is capable of simultaneously attending to all regions of an image, potentially providing advantages in the processing of complex integrated information. The hyperparameters and training process of the ViT model are provided in Supplementary Note 3 (http://links.lww.com/JS9/E191). Additionally, we employed the Inception v3 algorithm, commonly used in pathological deep learning models[27,28], for patch-level prediction to compare with the ViT model and select the optimal algorithm for subsequent analysis.

After training the ViT and Inception v3 models, we calculated the label for each patch and its corresponding prediction probability. The patch probability of optimal algorithm was then aggregated through multi-instance learning, resulting in a WSI-level prediction. The multi-instance learning for WSI-level prediction included Patch Likelihood Histogram (PLH) and Bag of Words (BoW) pipelines[29]. In PLH, we utilized a histogram to visualize the distribution of patch likelihood across the WSI, whereas in BoW, we mapped each patch to a Term Frequency-Inverse Document Frequency (TF-IDF) floating-point variable, and calculated a TF-IDF feature vector to represent the WSI. The results of PLH and BoW pipelines were ensembled to obtain the WSI-level prediction of each WSI for training conventional machine learning classifiers (LR, Extra Trees, Random Forest, Naive Bayes, SVM, KNN, XGBoost, and LightGBM). The selection strategies of features, optimal hyper-parameters, and optimal classifiers for the Pathology model were similar to the Habitat model.

Multi-modal integration and comparison

The selected clinical, habitat, and pathology features or signatures were used to construct the multi-modal models by a MHA model[25] and Ensemble method based on stacked machine learning models[30], respectively. The architecture of the MHA model and the Ensemble method are shown in Fig. 2b and 2c. The training of

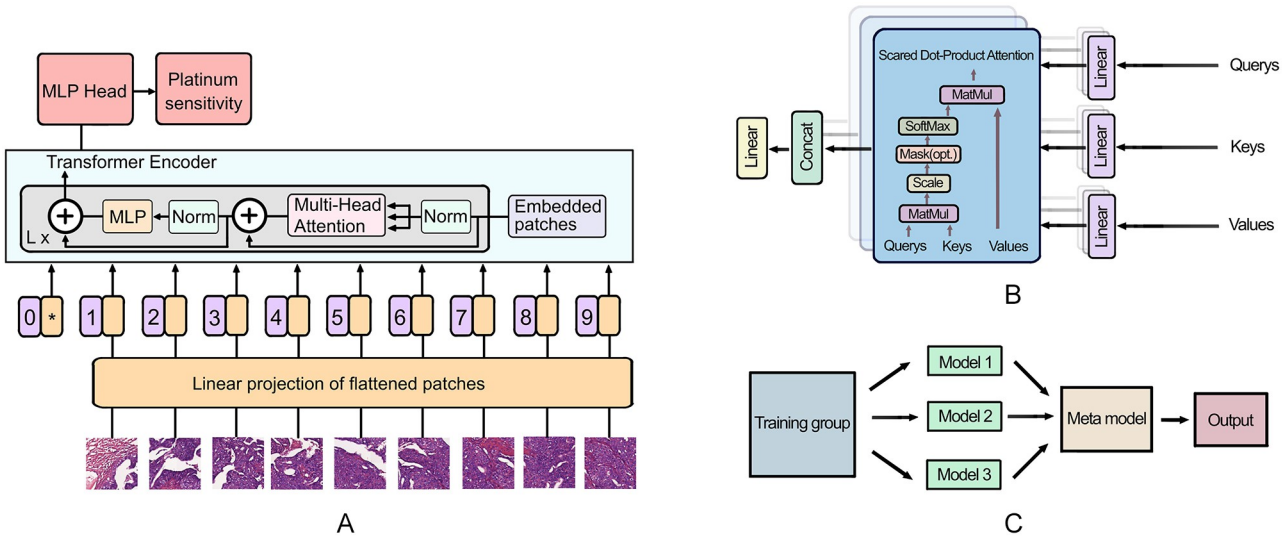

Figure 2. Various algorithm model architectures. (A) Vision transformer (B), multi-head attention (B), and ensemble method (C). The illustrations of the vision transformer and multi-head attention were respectively inspired by Dosovitskiy *et al* (2021) and Vaswani *et al* (2017).

the MHA model mainly included three steps. The first step was transformer encoding, which applied a multi-head self-attention mechanism to dynamically prioritize the most important features. The second step was feature fusion, the output of the encoder combined these processed features into a cohesive set that represented the comprehensive information from all the related images. Finally, these fused features were channeled into the classification layer to predict platinum sensitivity. The technical details of MHA multi-modal integration are provided in Supplementary Note 4 (http://links.lww.com/JS9/E191). To highlight the effectiveness of the MHA model, we also employed a commonly used late-fusion technique, Ensemble strategy, for multi-modal integration. The first layer of the Ensemble model was composed of CHP models, and the second layer takes the output of the first layer as the input of the multi-variate LR.

All eligible unimodal samples were included to evaluate the unimodal models, while the intersection set of patients was used to build the multi-modal models. When unimodal and multi-modal models were evaluated and compared together, only the patient intersections were analyzed. Receiver operating characteristic (ROC) curve with area under the curve (AUC), accuracy, sensitivity, specificity, positive predictive value, negative predictive value, and DeLong test were employed to evaluate and compare the discrimination performance. Additionally, integrated discrimination improvement (IDI) value was performed to assess model gains. The overall workflow of this study is exhibited in Fig. 3.

Statistical analysis

All statistical analyses were performed using SPSS software (version 26.0, IBM, New York, USA), Python (version 3.7.12, https://www.python.org/getit/), and OnekeyAI platform (https://github.com/onekeyAl-Platform/onekey). For continuous variables, we

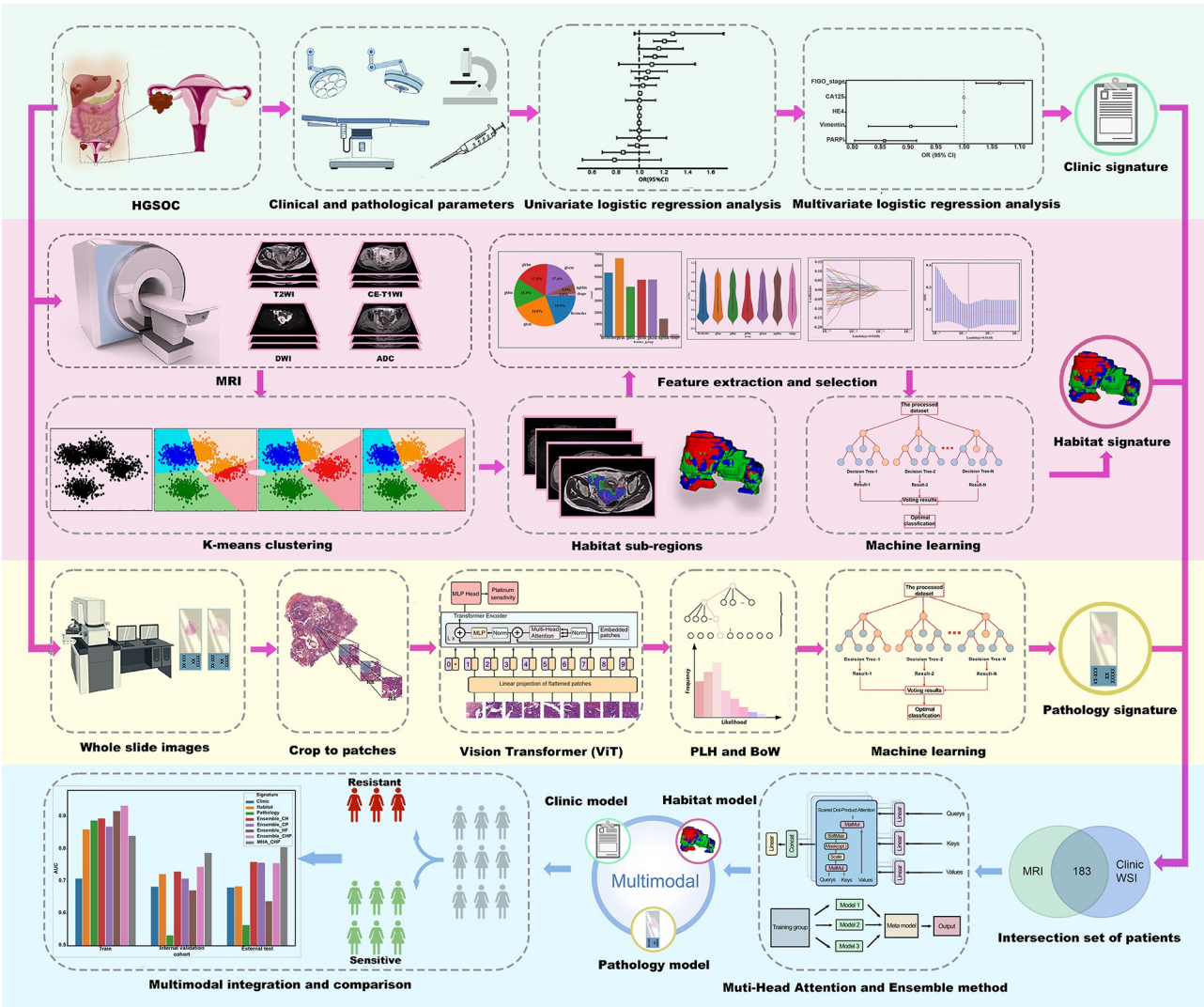

Figure 3. Workflow of the study. Preoperative MRI and postoperative H&E-stained WSIs of HGSOC patients were retrospectively collected. MRI habitat sub-regions were generated based on K-means clustering algorithm. After feature extraction and selection, three signatures (Habitat, Pathology, and Clinic) were constructed. Muti-head attention and ensemble method were used to construct multi-modal integration models. The performance of unimodal and multi-modal models in predicting platinum-resistant patients was validated and compared. T2WI: T2-weighted images; CE-T1WI: contrast-enhanced T1-weighted images; DWI: diffusion-weighted imaging; ADC: apparent diffusion coefficient; PLH: patch likelihood histogram; BoW: bag of words.

utilized the Kolmogorov–Smirnov test and *F*-test, respectively, to evaluate the normality of the distribution and variance homogeneity of the data, respectively. In cases where the data exhibited a normal distribution and had equal variance, the two-sample *t* test or analysis of variance (ANOVA) was employed to compare continuous variables; otherwise, the Mann–Whitney *U* test or Kruskal–Wallis *H* was conducted. The Pearson χ^2 test was used to compare the categorical variables. A $P < 0.05$ was considered a significant statistical difference. We have uploaded the main codes at https://github.com/fapingqaz/hcp.

Results

Baseline characteristics and Clinic model

A total of 754, 578, and 587 patients were incorporated to construct the unimodal CHP models, respectively. A total of 183 patients with simultaneous clinical, MRI, and WSI data were used to develop multi-modal models and compare them with unimodal models for the same sample size. The baseline clinicopathological characteristics in all cohorts (Supplementary Tables S2 and S3, http://links.lww.com/JS9/E191) show the comparison of the baseline characteristics distribution among the four models. Patients underwent NACT treatment only for constructing the MRI Habitat model, and not for building Clinic and Pathology models. There were some baseline clinicopathological characteristics with significant differences among the four models ($P < 0.05$). However, it did not affect the subsequent results, as we constructed the multi-modal model using the intersection of patients from these four models and compared it with the unimodal models using the same sample.

Univariate and multi-variate LR analyses of clinicopathological characteristics in the training cohort were displayed in Table 1. According to multi-variate LR analyses, poly ADP-ribose polymerase inhibitor (PARPi) maintenance therapy ($P<0.001$) and Federation of Gynecology and Obstetrics (FIGO) stage ($P = 0.013$) were clinically independent predictors for predicting platinum sensitivity in HGSOC patients. The AUCs of the unimodal Clinic model were 0.715, 0.674, and 0.661 in the training, validation, and test cohorts, respectively.

Habitat clustering and model construction

According to the Calinski–Harabasz score, the optimal number of clusters was four (Fig. 4a). Hence, one to four habitat sub-regions were classified in all tumors. A signal line plot of multi-parametric MRI at each habitat in all patients, as well as signal line plots of different habitats in platinum-sensitive and platinum-resistant patients on distinct sequences are shown in Fig. 4b–4f. Habitat 1 displayed moderate SI on almost all sequences. The strongest enhancement was observed in Habitat 2. Habitat 3 showed the highest SI on DWI, the lowest SI on ADC map, and moderate enhancement. On the contrary, Habitat 4 displayed the highest SI on ADC map and the lowest SI on CE-T1WI and DWI, belonging to the low-vascularity low-cellularity (LV-LC) habitat. Supplementary Table S4 (http://links.lww.com/JS9/E191) provides the mean SI, volume, and proportion of different habitats on multi-parametric MRI. The ADC SIs of Habitats 2 and 3 and the DWI SIs of Habitats 1 and 4 in platinum-sensitive patients were significantly lower than those in platinum-resistant patients (all $P < 0.05$). There were no significant differences in the volume and proportion of habitat sub-regions between

Table 1

Univariate and multi-variate LR analyses of clinicopathological characteristics in the training cohort for clinical analyses

	Univariate LR analysis			Multi-variate LR analysis		
	OR	OR 95%CI	*P*-value	OR	OR 95%CI	*P*-value
Age	0.999	0.995–1.002	0.557			
BMI	0.995	0.986–1.004	0.342			
CA125	1.000	1.000–1.000	0.012*	1.000	1.000–1.000	0.080
CA199	1.000	1.000–1.000	0.512			
CEA	1.000	0.998–1.002	0.929			
HE4	1.000	1.000–1.000	0.045*	1.000	1.000–1.000	0.211
PARPi	0.872	0.816–0.931	0.001*	0.857	0.803–0.915	<0.001*
Menopause	1.033	0.963–1.108	0.447			
Anemia	0.961	0.890–1.037	0.384			
FIGO stage	1.065	1.023–1.108	0.011*	1.064	1.021–1.107	0.013*
Bilateral lesions	1.021	0.954–1.092	0.618			
Residual tumor	0.975	0.913–1.042	0.536			
ER	1.013	0.898–1.143	0.863			
PR	1.002	0.907–1.107	0.977			
Ki-67	0.876	0.731–1.048	0.224			
P53	0.984	0.914–1.060	0.726			
P16	1.075	0.960–1.203	0.293			
WT-1	1.046	0.919–1.189	0.568			
CK7	0.891	0.670–1.186	0.508			
Vimentin	0.896	0.818–0.980	0.046*	0.905	0.829–0.987	0.059

LR: logistic regression; OR: odds ratio; CI: confidence interval; BMI: body mass index; CA125: cancer antigen 125; CA199: cancer antigen 199; CEA: carcino-embryonic antigen; HE4: human epididymis protein 4; NACT: neoadjuvant chemotherapy; PARPi: poly ADP-ribose polymerase inhibitor; FIGO: Federation of Gynecology and Obstetrics; R0: no macroscopic tumor; R1: the maximal diameter of residual tumor < 1cm; R2: the maximal diameter of residual tumor ≥ 1cm; ER: estrogen receptor; PR: progesterone receptor; P53: protein 53; P16: protein 16; WT-1: Wilms tumor protein-1; CK7: cytokeratin 7.
*P <0.05.

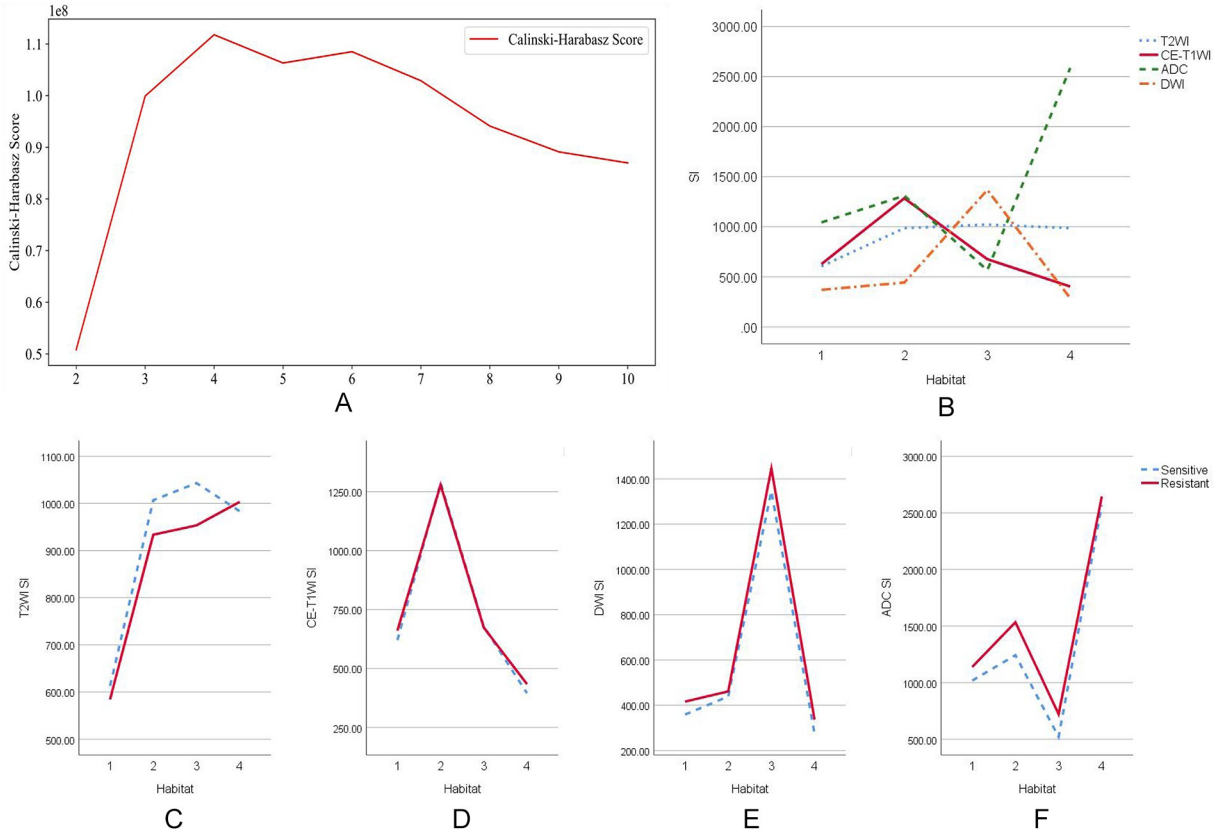

Figure 4. MRI habitat clustering. According to Calinski-Harabasz score line chart (A), the optimal number of clusters was determined to be four. A signal line plot of multi-parametric MRI at each habitat in all patients (B). Signal line plots of different habitats in platinum-sensitive and platinum-resistant patients on T2WI (C), CE-T1WI (D), DWI (E), and ADC maps (F).

the platinum-sensitive and platinum-resistant groups (all $P \geq 0.05$). The MRI and WSIs of representative cases are shown in Supplementary Figs. S2 and S3 (http://links.lww.com/JS9/E191).

After habitat feature extraction and selection, 32 features were retained to construct Habitat signature (Supplementary Fig. S1d, http://links.lww.com/JS9/E191). The optimal classifier to build the Habitat model was Random Forest based on the AUCs of the validation cohort and test cohort (Supplementary Table S5 and Fig. S4, http://links.lww.com/JS9/E191). For unimodal analysis, the AUCs of the Habitat model were 0.832, 0.721, and 0.707 in the training, validation, and test cohorts, respectively (Table 2).

Pathology model

Supplementary Table S6 (http://links.lww.com/JS9/E191) present the performance of ViT and Inception v3 models for patch-level prediction. In the internal validation cohort, the AUC of the ViT model (0.506) was higher than that of the Inception v3 model (0.477), while the opposite was true in the external test cohort.

Table 2

The performance of the unimodal models in their corresponding patient populations

	Models	AUC	Accuracy	Sensitivity	Specificity	PPV	NPV
Training cohort	Clinic	0.715	0.793	0.341	0.865	0.286	0.892
	Habitat	0.832	0.830	0.610	0.903	0.679	0.874
	Pathology	0.889	0.768	0.806	0.762	0.330	0.964
Internal validation cohort	Clinic	0.674	0.845	0.235	0.937	0.364	0.890
	Habitat	0.721	0.635	0.765	0.603	0.325	0.911
	Pathology	0.692	0.576	0.800	0.544	0.203	0.949
External test cohort	Clinic	0.661	0.844	0.140	0.951	0.300	0.879
	Habitat	0.707	0.709	0.667	0.716	0.268	0.932
	Pathology	0.700	0.879	0.360	1.000	1.000	0.870

AUC: area under the curve; PPV: positive predictive value; NPV: negative predictive value.

Considering the AUC of the training cohort (0.837), we selected ViT as the optimal algorithm for subsequent analysis, as the Inception v3 model exhibited overfitting. Supplementary Table S7 and Fig. S4 (http://links.lww.com/JS9/E191) show the performance of different classifiers for WSI-level prediction in the Pathology model. On the basis of the AUCs in the validation cohort and test cohort, the optimal classifier to build the Pathology model was Random Forest. For unimodal analysis, the AUCs of the Pathology model were 0.889, 0.692, and 0.700 in the training, validation, and test cohorts, respectively (Table 2).

Multi-modal integration and comparison

Table 3 shows the prediction performance of the different models in the intersection set of patients. Figure 5 exhibits the ROC curves and heatmaps of IDI values. The AUC histograms of different models and heatmaps of DeLong test are presented in Supplementary Fig. S5 (http://links.lww.com/JS9/E191). When the patient intersection was compared, the AUCs of the Habitat model (0.722 and 0.685) were higher than those of the Clinic model (0.683 and 0.681) and the Pathology model (0.533 and 0.565) in both the internal validation cohort and the external test cohort. The AUCs of the CHP model based on MHA (MHA_CHP model) in the validation (0.789) and test cohorts (0.807) were highest among all unimodal and multi-modal models. Except the Habitat and Pathology (HP) model based on the Ensemble method (Ensemble_HP), the AUCs of other Ensemble models were higher than those of unimodal models in the validation and test cohorts. Although Delong test showed no significant differences in the performance between each model in the validation and test cohorts (all $P > 0.05$), compared with other models, the IDI values of the MHA_CHP model were positive compared with other models.

Discussion

In this study, we applied K-means clustering algorithm to perform habitat imaging on multi-parameter MRI and integrated it with WSI to establish multi-scale comprehensive models for predicting platinum sensitivity in HGSOC patients. We found PARPi maintenance therapy and FIGO stage were clinically independent predictors for predicting platinum sensitivity. The SIs of habitat sub-regions on DWI or ADC maps were associated with platinum resistance. The CHP models had some potentials to predict platinum resistance of HGSOC patients when unimodal models were developed with the corresponding patient population. When the patient intersection was compared, the AUCs of the Habitat model were higher than those of the Clinic and Pathology models. The performance of the MHA_CHP model was the highest among all models, and most Ensemble models outperformed unimodal models. This study may potentially assist clinicians in accurately predicting the efficacy of platinum-based chemotherapy in HGSOC patients before treatment, which is crucial for the development of patient-specific treatment plans and the optimization of comprehensive patient management.

At present, the widely used ovarian staging system is the FIGO staging system in 2014[31], which was also adopted in this study. And we found that FIGO stage was one of the clinically independent predictors for predicting platinum sensitivity in HGSOC patients. The higher the probability of

Table 3

The performance of the different models in the intersection set of patients

	Models	AUC	Accuracy	Sensitivity	Specificity	PPV	NPV
Training cohort	Clinic	0.708	0.757	0.389	0.828	0.304	0.875
	Habitat	0.861	0.847	0.722	0.871	0.520	0.942
	Pathology	0.888	0.820	0.778	0.828	0.467	0.951
	Ensemble_CH	0.895	0.802	0.778	0.806	0.437	0.949
	Ensemble_CP	0.869	0.838	0.722	0.860	0.500	0.941
	Ensemble_HP	0.918	0.847	0.833	0.849	0.517	0.963
	Ensemble_CHP	0.934	0.847	0.833	0.849	0.517	0.963
	MHA_CHP	0.841	0.739	0.778	0.731	0.359	0.944
Internal validation cohort	Clinic	0.683	0.878	0.000	1.000	0.000	0.878
	Habitat	0.722	0.683	0.600	0.694	0.214	0.926
	Pathology	0.533	0.293	0.800	0.222	0.125	0.889
	Ensemble_CH	0.731	0.756	0.600	0.778	0.273	0.933
	Ensemble_CP	0.708	0.634	0.600	0.639	0.187	0.920
	Ensemble_HP	0.672	0.610	0.800	0.583	0.211	0.955
	Ensemble_CHP	0.744	0.756	0.600	0.778	0.273	0.933
	MHA_CHP	0.789	0.585	0.800	0.556	0.200	0.952
External test cohort	Clinic	0.681	0.613	0.214	0.941	0.750	0.593
	Habitat	0.685	0.710	0.643	0.765	0.692	0.722
	Pathology	0.565	0.613	0.143	1.000	1.000	0.586
	Ensemble_CH	0.761	0.742	0.643	0.824	0.750	0.737
	Ensemble_CP	0.758	0.710	0.571	0.824	0.727	0.700
	Ensemble_HP	0.639	0.645	0.571	0.706	0.615	0.667
	Ensemble_CHP	0.756	0.742	0.571	0.882	0.800	0.714
	MHA_CHP	0.807	0.742	0.500	0.941	0.875	0.696

CH: Clinic and Habitat; CP: Clinic and Pathology; HP: Habitat and Pathology; CHP: Clinic, Habitat, and Pathology; MHA: multi-head attention.

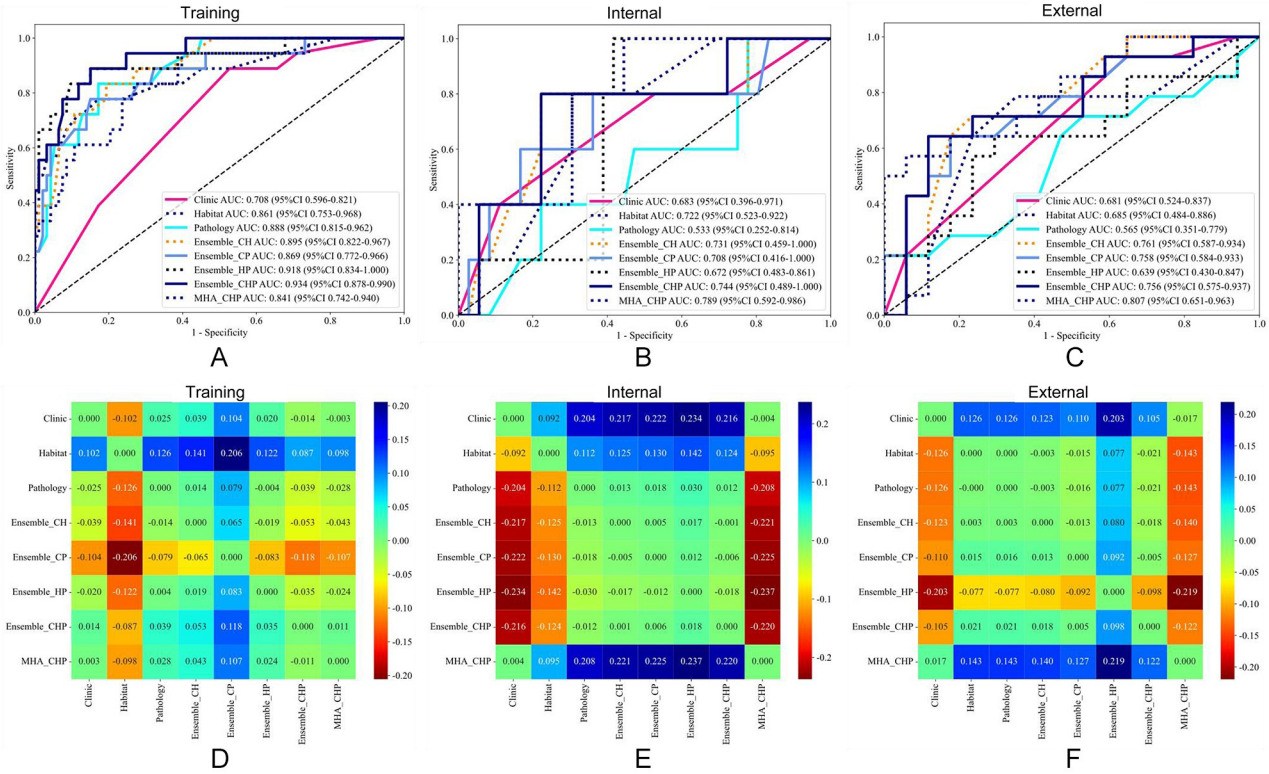

Figure 5. Comparison and evaluation of different models. Receiver operating characteristic curves (A, B, and C) and IDI heatmaps (D, E, and F) of different models in the training cohort (A and B), internal validation cohort (B and E), and external test cohort (C and F). The Muti-Head Attention models combined with clinical, habitat, and pathological data (MHA_CHP) showed the highest AUCs in both the internal validation cohort (0.789) and the external test cohort (0.807). Compared with other models, the IDI values of MHA_CHP models in the internal validation cohort and the external test cohort were positive.

postoperative residual in patients with advanced stage, the worse the effect of platinum-based chemotherapy, which was consistent with the findings of Li *et al*[9]. A high-level evidence indicates that frontline PARPi maintenance therapy has become the standard for patients with advanced OC after initial treatment, and is better able to delay recurrence and improve patient outcomes[32]. Therefore, PARPi maintenance therapy may reduce the occurrence of platinum resistance in patients by reducing patient relapse. Nevertheless, rigorous randomized controlled trials are needed to confirm this hypothesis. For decades, NACT has been regarded as the standard treatment for advanced OC, especially among patients who are not suitable for primary debulking surgery[33]. However, NACT carries a potential risk of inducing platinum resistance[34]. Notably, we only included patients who underwent primary debulking surgery (i.e., without NACT) in the Clinic and Pathology models. Because the WSIs after NACT does not represent the pathological state of the lesions at baseline, so patients after NACT need to be excluded when constructing the Pathology model. Similarly, multi-modal models need to be constructed in the intersection of patients with clinical, MRI, and pathological data, and NACT is likely to become an independent predictor of platinum resistance, so the Clinic model also needs to exclude patients with NACT. According to multi-variate LR analysis, the predictive performance of the Clinic model was not good in our study. One possible reason was the non-determinacy of clinical predictors, that is, the latest clinical practice guidelines did not recommend definitive clinical markers that accurately predict platinum resistance of OC[4]. Additionally, uneven distribution of some clinical and pathological features between the training cohort and the test cohort also compromise model performance. Therefore, it is necessary to find alternative effective biomarkers for predicting platinum sensitivity.

Previous evidence indicated that intratumoral heterogeneity was related to the treatment response of tumors[35]. Habitat imaging is a novel cancer imaging approach that identifies tumor sub-regions based on similar imaging features. It can noninvasively evaluate tumor heterogeneity and characterize the alterations of tumor microenvironment[36,37]. Emerging data indicated that MRI-based habitat imaging contributed to predicting chemotherapy response and assessing platinum resistance of tumors[38,39]. In this study, we clustered four habitats and found that the ADC SI of the platinum sensitive group was significantly lower than that of the platinum resistant group. According to the SIs on different sequences, the solid components were dominant at Habitat 3. In other words, the cell density of solid components in platinum-sensitive patients might be higher than that in platinum-resistant patients. Itamochi *et al*[40] considered the high resistance of OC to chemotherapy was relevant to the low proliferation rate of ovarian tumor cells. Low-proliferation tumor cells are characterized by low cell density, less diffusion restriction of water molecules, and high ADC values. Hence, the results of their study supported our findings from another aspect. In addition, our study also

found that Habitat 4 (LV-LC habitat) was associated with platinum resistance. Kazerouni *et al*[37] suggested that the presence of LV-LC habitat resulted in reduced tumor sensitivities for chemotherapy, which was consistent with our results. Nevertheless, the biological implications of habitat imaging are subjective. It is necessary to construct effective models to predict platinum resistance in HGSOC patients.

A recent study attempted to use MRI-based habitat radiomics to predict platinum resistance in HGSOC patients, with an unremarkable AUC of 0.710[41]. In this study, we found the prediction performance of the habitat model was also not superior, indicating that the radiological information of habitat subregions at the macroscale was not enough to fully interpret the tumor microenvironment of HGSOC. In certain circumstances, compared with the macroscopic information obtained from multi-parametric MRI, the pathological information observed under a microscope is important for a comprehensive description of the lesions[42]. The unimodal Pathology model showed moderate performance for predicting platinum resistance of HGSOC in our study. Lan *et al*[19] considered a low cancer cell ratio as well as high stromal cell ratio were significantly correlated with high frequency of platinum-resistant recurrence, which was in alignment with our study. It is known that platinum-based drugs slow tumor cell proliferation mainly by preventing DNA replication, sparse tumor cells often have inactive DNA replication, making them somewhat to be tolerant to platinum-based drugs[43]. When the intersection set of patients was used for model comparison, the AUC of the Pathology model decreased, suggesting possible sample bias, which needs to be further verified by increasing the sample size. In addition, we found that the sensitivity of the Pathology model in the external validation cohort was low. On one hand, pathomics models are usually trained based on features from specific datasets, and if the external data contains untrained tissue variations (such as areas of inflammation or fibrosis), the sensitivity may significantly decrease[44]. On the other hand, single-slide analysis may miss key lesion areas, especially in early disease or focal pathological changes, which can also lead to reduced sensitivity[45]. In actual clinical scenarios, the limitations of puncture biopsy samples may further amplify such issues. Therefore, the current Pathology model is more suitable as auxiliary tools rather than being used independently for diagnosis. Future prospective clinical trials are needed to validate its robustness in the real world and to establish a collaborative workflow with traditional pathological diagnosis.

The biological characteristics of tumors are intricate and influenced by numerous factors, so assessing the effectiveness of treatment necessitates the integration of multi-scale data[46]. The multi-modal integration of medical imaging and histopathology for guiding oncologic decision-making is still in its infancy[47]. A series of recent high-quality studies showed that multi-modal integration including radiology and pathology effectively improved the prediction performance of treatment response and prognosis in tumor patients[20,48,49]. In this study, the predictive performance of platinum sensitivity using the multi-scale models was almost better than that using the unimodal models alone. Habitat reflected voxel signal intensity distributions and spatial heterogeneity of tumor at macroscale in vivo; pathology provided details of tissue structures and cell types at microscale in vitro; and clinical predictors offered information reflecting body function at the host level. How to better integrate these multi-modal data of different scales has gradually become a challenge. Vanguri *et al*[48] conducted multi-omics fusion of CT, pathology, and genomic based on an attention mechanism, and found that this integrated model could more accurately predict the immunotherapy efficacy in patients with non-small cell lung cancer. We also found that the performance of the MHA_CHP model was the highest among all models. The possible explanation is that the multi-modal integration obtained from the individual level to the cellular level plays a complementary role in assessing platinum sensitivity. Meanwhile, MHA can not only provide more comprehensive information compared with existing convolutional neural network, but also efficiently utilize useful information from each model at different scales, aiming to obtain high-level context features and effectively complement the target model[21]. Therefore, the MHA-based multi-modal model can effectively improve the prediction performance.

This study had some limitations. First, our dataset was retrospectively collected from four hospitals, and not all patients were available for MRI and WSI data, leading to a limited number of patients enrolled in multi-modal models. Further prospective studies with a larger sample size from more centers are warranted. Second, the image segmentation was performed by two radiologists in consensus due to the large size and extensive distribution of lesions, thus we did not evaluate the interobserver and intraobserver consistencies. It is necessary to develop an automatic segmentation strategy to improve the speed and stability of image segmentation. Third, WSIs were derived from tumor focal samples of patients after surgery, and there might be sampling bias and tissue heterogeneity. Further prospective studies should conduct point-to-point correlation analyses between preoperative MRI habitats and postoperative WSIs.

In conclusion, PARPi maintenance therapy and FIGO stage were clinically independent predictors for predicting platinum sensitivity. Habitat imaging based on MRI was associated with platinum sensitivity in HGSOC patients. The unimodal Habitat and Pathology models demonstrated the same potential to predict platinum resistance, with a superior performance to the Clinic models. The MHA_CHP model successfully predicted the platinum sensitivity and exhibited higher and more stable predictive performance than other models. This study is promising for integrating multi-modal data based on MHA and future models using larger sample sizes will make it possible to provide clinicians with therapeutic strategies and augment the effectiveness of individual treatments.

Ethical approval

This retrospective study was approved by the institutional research committee of the First People's Hospital of Yunnan Province (reference number: KHLL2023-KY208), and patients' written informed consents were waived.

Consent

This was a retrospective study, the ethics review passed the informed consent exemption, we protect the privacy rights of patients' and Patients' and volunteers' names, initials, or hospital numbers were not used.

Sources of funding

This study was supported by the National Natural Science Foundations of China (82460340, 82471943, 82471932, 82271940, and 82160524); the Yunnan Health Training Project of High Level Talents (H-2024080); the Kunming University of Science and Technology and the First People's Hospital of Yunnan Province Joint Special Project on Medical Research (KUST-KH2022027Y); the Basic Research on Application of Joint Special Funding of Science and Technology Department of Yunnan ProvinceKunming Medical University (202301AY070001-084); the Shanghai Jinshan District Health Committee (SZK2023A02), and the Natural Science Foundation of Shanghai (22ZR1412500).

Author contributions

Q.B.: conceptualization, funding acquisition; methodology, validation; writing – original draft. C.H.A.: data curation, funding acquisition, investigation, resources. Q.Y.M., Q.Q.W.: data curation, investigation,; resources. H.Y.L., A.Z., W.W.S., Y.L.: data curation. Y.Z.W.: formal analysis. Y.S.: software, visualization. Z.B.X.: data curation, resources, supervision. H.M.L.: conceptualization, funding acquisition, writing – review and editing. J.W.Q.: project administration, supervision, writing – review and editing, funding acquisition.

Conflicts of interest disclosure

The authors declare no competing interests.

Research registration unique identifying number (UIN)

UIN: NCT06787170.

Guarantor

Jinwei Qiang.

Provenance and peer review

Not commissioned, externally peer-reviewed.

Data availability statement

The datasets used and analyzed during the present study are available from the corresponding author on reasonable request.

Assistance with the study

None.

Presentation

None.

References

[1] Siegel RL, Giaquinto AN, Jemal A. Cancer statistics, 2024. CA Cancer J Clin 2024;74:12–49.
[2] Barnes BM, Nelson L, Tighe A, *et al*. Distinct transcriptional programs stratify ovarian cancer cell lines into the five major histological subtypes. Genome Med 2021;13:140.
[3] Folsom SM, Berger J, Soong TR, Rangaswamy B. Comprehensive review of serous tumors of tubo-ovarian origin: clinical behavior, pathological correlation, current molecular updates, and imaging manifestations. Curr Probl Diagn Radiol 2023;52:425–38.
[4] Gonzalez-Martin A, Harter P, Leary A, *et al*. Newly diagnosed and relapsed epithelial ovarian cancer: ESMO Clinical Practice Guideline for diagnosis, treatment and follow-up. Ann Oncol 2023;34:833–48.
[5] Lheureux S, Gourley C, Vergote I, Oza AM. Epithelial ovarian cancer. Lancet 2019;393:1240–53.
[6] Le Saux O, Ray-Coquard I, Labidi-Galy SI. Challenges for immunotherapy for the treatment of platinum resistant ovarian cancer. Semin Cancer Biol 2021;77:127–43.
[7] Winfield JM, Wakefield JC, Brenton JD, *et al*. Biomarkers for site-specific response to neoadjuvant chemotherapy in epithelial ovarian cancer: relating MRI changes to tumour cell load and necrosis. Br J Cancer 2021;124:1130–37.
[8] Winfield JM, Wakefield JC, Dolling D, *et al*. Diffusion-weighted MRI in advanced epithelial ovarian cancer: apparent diffusion coefficient as a response marker. Radiology 2019;293:374–83.
[9] Li H, Cai S, Deng L, *et al*. Prediction of platinum resistance for advanced high-grade serous ovarian carcinoma using MRI-based radiomics nomogram. Eur Radiol 2023;33:5298–308.
[10] Lei R, Yu Y, Li Q, *et al*. Deep learning magnetic resonance imaging predicts platinum sensitivity in patients with epithelial ovarian cancer. Front Oncol 2022;12:895177.
[11] Li Y, Jian J, Ge H, Gao X, Qiang J. Peritumoral MRI radiomics features increase the evaluation efficiency for response to chemotherapy in patients with epithelial ovarian cancer. J Magn Reson Imaging 2024;60:2718–27.
[12] Tomaszewski MR, Gillies RJ. The biological meaning of radiomic features. Radiology 2021;298:505–16.
[13] Napel S, Mu W, Jardim-Perassi BV, Aerts H, Gillies RJ. Quantitative imaging of cancer in the postgenomic era: radio(geno)mics, deep learning, and habitats. Cancer 2018;124:4633–49.
[14] O'Connor JP, Rose CJ, Waterton JC, Carano RA, Parker GJ, Jackson A. Imaging intratumor heterogeneity: role in therapy response, resistance, and clinical outcome. Clin Cancer Res 2015;21:249–57.
[15] Wang X, Xu C, Grzegorzek M, Sun H. Habitat radiomics analysis of PET/CT imaging in high-grade serous ovarian cancer: application to Ki-67 status and progression-free survival. Front Physiol 2022;13:948767.
[16] Holscher DL, Bouteldja N, Joodaki M, *et al*. Next-generation morphometry for pathomics – data mining in histopathology. Nat Commun 2023;14:470.
[17] Ahn B, Moon D, Kim HS, *et al*. Histopathologic image-based deep learning classifier for predicting platinum-based treatment responses in high-grade serous ovarian cancer. Nat Commun 2024;15:4253.
[18] Bergstrom EN, Abbasi A, Diaz-Gay M, *et al*. Deep learning artificial intelligence predicts homologous recombination deficiency and platinum response from histologic slides. J Clin Oncol 2024;42:3550–60.
[19] Lou E, Clemente V, Grube M, *et al*. Tumor-stroma proportion to predict chemoresistance in patients with ovarian cancer. JAMA Network Open 2024;7:e240407.
[20] Boehm KM, Aherne EA, Ellenson L, *et al*. Multimodal data integration using machine learning improves risk stratification of high-grade serous ovarian cancer. Nat Cancer 2022;3:723–33.
[21] Feng CM, Yan Y, Chen G, *et al*. Multimodal transformer for accelerated MR imaging. IEEE Trans Med Imaging 2023;42:2804–16.
[22] Bossuyt PM, Reitsma JB, Bruns DE, *et al*. STARD 2015: an updated list of essential items for reporting diagnostic accuracy studies. BMJ 2015;351:h5527.
[23] Wang T, Tang J, Yang H, *et al*. Effect of apatinib plus pegylated liposomal doxorubicin vs pegylated liposomal doxorubicin alone on platinum-resistant recurrent ovarian cancer: the approve randomized clinical trial. JAMA Oncol 2022;8:1169–76.
[24] Macenko M, Niethammer M, Marron JS, *et al*. A method for normalizing histology slides for quantitative analysis. IEEE Int Symp Biomed Imaging. 2009;1107–10.
[25] Vaswani A, Shazeer N, Parmar N, *et al*. Attention is all you need. 2017. arXiv:1706.03762.

[26] Dosovitskiy A, Beyer L, Kolesnikov A, *et al*. An image is worth 16x16 words: transformers for image recognition at scale. 2021. arXiv:2010.11929.
[27] Coudray N, Ocampo PS, Sakellaropoulos T, *et al*. Classification and mutation prediction from non-small cell lung cancer histopathology images using deep learning. Nat Med 2018;24:1559–67.
[28] Cai X, Zhang H, Wang Y, Zhang J, Li T. Digital pathology-based artificial intelligence models for differential diagnosis and prognosis of sporadic odontogenic keratocysts. Int J Oral Sci 2024;16:16.
[29] Cao R, Yang F, Ma SC, *et al*. Development and interpretation of a pathomics-based model for the prediction of microsatellite instability in colorectal cancer. Theranostics 2020;10:11080–91.
[30] Naimi AI, Balzer LB. Stacked generalization: an introduction to super learning. Eur J Epidemiol 2018;33:459–64.
[31] Prat J. Staging classification for cancer of the ovary, fallopian tube, and peritoneum. Int J Gynaecol Obstet 2014;124:1–5.
[32] Tew WP, Lacchetti C, Ellis A, *et al*. PARP inhibitors in the management of ovarian cancer: ASCO guideline. J Clin Oncol 2020;38:3468–93.
[33] Armstrong DK, Alvarez RD, Bakkum-Gamez JN, *et al*. Ovarian cancer, version 2.2020, NCCN clinical practice guidelines in oncology. J Natl Compr Canc Netw 2021;19:191–226.
[34] Liu J, Jiao X, Gao Q. Neoadjuvant chemotherapy-related platinum resistance in ovarian cancer. Drug Discov Today 2020;25:1232–38.
[35] Koren S, Bentires-Alj M. Breast tumor heterogeneity: source of fitness, hurdle for therapy. Mol Cell 2015;60:537–46.
[36] Waqar M, Van Houdt PJ, Hessen E, *et al*. Visualising spatial heterogeneity in glioblastoma using imaging habitats. Front Oncol 2022;12:1037896.
[37] Kazerouni AS, Hormuth DN, Davis T, *et al*. Quantifying tumor heterogeneity via MRI habitats to characterize microenvironmental alterations in HER2+ breast cancer. Cancers (Basel) 2022;14:1837.
[38] Jeong SY, Park JE, Kim N, Kim HS. Hypovascular cellular tumor in primary central nervous system lymphoma is associated with treatment resistance: tumor habitat analysis using physiologic MRI. AJNR Am J Neuroradiol 2022;43:40–47.
[39] Shi Z, Huang X, Cheng Z, *et al*. MRI-based quantification of intratumoral heterogeneity for predicting treatment response to neoadjuvant chemotherapy in breast cancer. Radiology 2023;308:e222830.
[40] Itamochi H, Kigawa J, Sugiyama T, Kikuchi Y, Suzuki M, Terakawa N. Low proliferation activity may be associated with chemoresistance in clear cell carcinoma of the ovary. Obstet Gynecol 2002;100:281–87.
[41] Bi Q, Miao K, Xu N, *et al*. Habitat radiomics based on MRI for predicting platinum resistance in patients with high-grade serous ovarian carcinoma: a multicenter study. Acad Radiol 2024;31:2367–80.
[42] Shao L, Liu Z, Feng L, *et al*. Multiparametric MRI and whole slide image-based pretreatment prediction of pathological response to neoadjuvant chemoradiotherapy in rectal cancer: a multicenter radiopathomic study. Ann Surg Oncol 2020;27:4296–306.
[43] Itamochi H, Kigawa J, Terakawa N. Mechanisms of chemoresistance and poor prognosis in ovarian clear cell carcinoma. Cancer Sci 2008;99:653–58.
[44] Valkonen M, Ruusuvuori P, Kartasalo K, Nykter M, Visakorpi T, Latonen L. Analysis of spatial heterogeneity in normal epithelium and preneoplastic alterations in mouse prostate tumor models. Sci Rep 2017;7:44831.
[45] Haubruck P, Heller R, Blaker CL, *et al*. Streamlining quantitative joint-wide medial femoro-tibial histopathological scoring of mouse post-traumatic knee osteoarthritis models. Osteoarthritis Cartilage 2023;31:1602–11.
[46] Saltz J, Almeida J, Gao Y, *et al*. Towards generation, management, and exploration of combined radiomics and pathomics datasets for cancer research. AMIA Jt Summits Transl Sci Proc 2017;2017:85–94.
[47] Boehm KM, Khosravi P, Vanguri R, Gao J, Shah SP. Harnessing multimodal data integration to advance precision oncology. Nat Rev Cancer 2022;22:114–26.
[48] Vanguri RS, Luo J, Aukerman AT, *et al*. Multimodal integration of radiology, pathology and genomics for prediction of response to PD-(L)1 blockade in patients with non-small cell lung cancer. Nat Cancer 2022;3:1151–64.
[49] Feng L, Liu Z, Li C, *et al*. Development and validation of a radiopathomics model to predict pathological complete response to neoadjuvant chemoradiotherapy in locally advanced rectal cancer: a multicentre observational study. Lancet Digit Health 2022;4:e8–e17.